Fisheries Oceanography
Volume 16 Issue 6 Page 489-505, November 2007
http://dx.doi.org/ 10.1111/j.1365-2419.2007.00443.x

Biophysical modelling of larval drift, growth and survival for the prediction of anchovy (*Engraulis encrasicolus*) recruitment in the Bay of Biscay (NE Atlantic)

Gwenhael Allain [1] Pierre Petitgas [1,*] Pascal Lazure [2] And Patrick Grellier [1]

1IFREMER, BP 21105, F- 44311 cedex 03, Nantes, France
2IFREMER, BP 70, F- 29280, Plouzané, France

*Correspondence. e-mail : Pierre.Petitgas@ifremer.fr
phone : +33 240 37 40 00
fax : +33 240 37 40 75

Abstract:

Fish recruitment is the result of the integration over a season and large oceanic areas of small-scale processes affecting larval survival. A hydrodynamic model was used (a) to explore and model these physical-biological interaction mechanisms and then (b) to perform the integration from individual to population scales in order to provide recruitment predictions for fisheries management. This method was applied to the case of anchovy (*Engraulis encrasicolus*) in the Bay of Biscay (NE Atlantic). (a) To tackle survival mechanisms, the main data available were past growth (otolith) records of larvae and juveniles sampled at sea. The drift history of these individuals was reconstructed by a backtracking procedure using hydrodynamic simulations. Along the individual trajectories obtained, the relationships between (real) growth variation and variations in physical parameters (estimated by hydrodynamic simulations) were explored. These relationships were then used to build and adjust individual-based growth and survival models. (b) Thousands of virtual buoys were released in the hydrodynamic model in order to reproduce the space-time spawning dynamics. Along the buoy trajectories (representative of sub-cohorts), the biophysical model was run to simulate growth and survival as a function of the environment encountered. The survival rate after three months of drift was estimated for each sub-cohort. The sum of all these survival rates over the season constituted an annual recruitment index. This index was validated over a series of recruitment estimations. The modelling choices, model results and potential use of the recruitment index for fisheries management are discussed.

Keywords : physical-biological interactions, individual-based models, recruitment, anchovy, Biscay

1. INTRODUCTION

A common feature of fish stocks collapses in history has been the conjunction over a time period of intense fishing effort and succession of low recruitments due to unfavorable environmental conditions (Larkin 1996). The population dynamics of short-lived species such as small pelagics is especially dependent on recruitment success. More generally, exploitation tends to reduce the life expectancy of all targeted fish populations and consequently increase their dependence on annual recruitment (Longhurst, 1988). The objective of recruitment prediction requires fisheries oceanography tools to detect environmental variations and their impact on fish populations. A first approach has consisted in establishing large-scale correlations between fish abundance and climate variables (Shepherd *et al*., 1984). Most of these correlation models worked for some time then failed, revealing a generally low reliability of this type of pattern oriented approach in which recruitment processes remained largely implicit (Myers, 1998). Such correlative approach has also been applied to anchovy recruitment (*Engraulis encrasicolus*) in the Bay of Biscay where the international fishery (Spain and France) is strongly dependent on annual recruitment. Recruitment indices based on winds (Borja *et al*., 1996) then on meso-scale ocean processes (Allain *et al*., 2001) were used by ICES for projecting the population one year in advance with ambivalent results (good estimation of low recruitment, underestimation of high recruitments: ICES, 2004).

Recruitment is the result of the integration over a season and large oceanic areas of processes affecting larval survival, which are dependent on small-scale mechanisms. Opposite to the pattern-oriented approach, process-oriented studies and models have been developed in fisheries science. Small-scale mechanisms influent on larval mortality were studied in detail in both laboratory and field experiments (Chambers and Trippel, 1997). The results of these studies were integrated into a variety of models, especially individual-based models (DeAngelis and Gross, 1992). Interactions between physics, planktonic prey and larvae were simulated in a deterministic way in individual-based models coupled to hydrodynamic models allowing drift and mortality simulations (Megrey *et al*., 1996; Lynch *et al*., 1996; Heath and Gallego, 1997; Bartsch and Coombs, 2001, 2004; Mullon *et al*., 2003). These individual-based ecological models, adapted to the study of recruitment mechanisms and to detailed sensitivity analyses, were not used for prediction purposes at the population scale or did not ameliorate prediction reliability, due to their complexity and the difficulty to estimate a number of biological variables at small scale over large ocean areas (Hinckley *et al*., 2000 ; Hermann *et al*., 2001). Considering the lack of knowledge and uncertainties about a number of processes, de Young *et al*. (2004) highlighted the need for taking into account the uncertainties and suggested probabilistic simulations.

The objective of this paper was to build a recruitment model that would be close enough to explicit mechanisms to be more reliable than correlation models and simple enough to be used for prediction. Such an approach required to perform the integration from individual scale (*i.e*. the scale of mechanisms) to population scale (the scale of annual result). A hydrodynamic circulation model was used for performing this integration.

To tackle survival mechanisms, the main data available were past growth (otolith) records of larvae and juveniles sampled at sea. The drift history of these individuals was reconstructed by a backtracking procedure using hydrodynamic simulations. Along the individual trajectories obtained, the relationships between (real) growth variation and variations in physical parameters (estimated by hydrodynamic simulations) were explored. These relationships were then used to build and adjust individual-based growth and survival statistical models. Thousands of virtual buoys were then released in the hydrodynamic model in order to reproduce the space-time spawning dynamics. Along the buoy trajectories (representative of sub-cohorts), the biophysical model was run to simulate growth and survival as a function of the environment encountered. The survival rate after 100 days of drift was estimated for each sub-cohort. The sum of all these survival rates over the season constituted an annual recruitment index, which values were compared to the series of recruitment estimations made by ICES. A schematic diagram summarizes the procedure followed (Fig. 1).

2. MATERIALS AND METHODS

2.1. Determination of birth dates and growth curves by otolith microstructure analysis

In spring 1999, monthly egg and larval surveys were undertaken by IFREMER from April to July on a major spawning ground of anchovy off Gironde estuary (Fig. 2). In September 1999, an acoustic survey targeting juvenile anchovies was jointly conducted by IFREMER and AZTI in SE Biscay, Spanish coast and continental shelf off Gironde (Fig. 2), areas known as potential nursery grounds (Uriarte *et al.,* 1996). 102 larvae and 148 juveniles were analysed. The thin otoliths (sagittae) of the larvae were read directly using a light microscope at magnification x1250. The thicker otoliths (sagittae) of the juveniles had to be polished before reading. Ototlith increments of larval and juvenile anchovy are deposited on a daily basis (Cermeno *et al*., 2003). The age of each individual was counted in daily increments from the mark of mouth opening (Campana and Jones, 1992). Subsequently we will use "hatch date" or "date of mouth opening" equally. The hatch date was then deduced from the estimated age and the sampling date. Otolith width was measured every five increments from the inner-most increment to the edge of the otolith. Growth rate (mm day^{-1}) was defined as the measured otolith width divided by the number of daily increments corresponding to the measured width. Otolith growth was adopted as a proxy measurement for somatic growth (Garcia *et al*., 1998; Palomera et al., 1988; Ré, 1986). The assumption of proportionality between otolith growth and somatic growth was verified by the strong relationship between standard length and sagitta radius. For details on the surveys and otolith microstructure analyses, see Allain *et al.* (2003).

2.2. Reconstruction of drift trajectories by a back-tracking procedure in a hydrodynamic model

A 3D circulation model (MARS3D) for the whole Bay of Biscay (Allain *et al*., 2003; Jégou *et al*., 2001; Lazure and Jégou, 1998) was developed at IFREMER, which extended from the French coast at the eastern limit to 8°W and from the Spanish coast at the southern limit to 49°N. The numerical grid had a 5 km x 5 km resolution in the horizontal plane and 30 sigma levels in the vertical. The time step was approximately 900 seconds corresponding to a fixed portion of the tidal cycle. The open boundary conditions (sea level elevation and currents) were produced by a larger 2D barotropic model extending from Portugal to Iceland which was forced by the semi-diurnal tide and by wind fields. Winds estimated by Météo-France ARPEGE model were used as a surface condition and a radiation condition was used for sea water temperature. Daily run-off of the Loire, Gironde and Adour rivers were used as boundary conditions. The temperature and salinity fields calculated by the model were validated by comparison with survey data and with satellite observations (Jégou *et al*., 2001).
Anchovy larvae and juveniles were found in the surface layer (0-30 m) mainly above the thermocline during surveys. Anchovy larvae were reported to carry out daily vertical migrations (Palomera, 1991, Garcia *et al*., 1998). Therefore we considered the upper 30 m layer as representative of the habitat of anchovy larvae and juveniles. The upper 30 m layer was a water mass that was tracked in the hydrodynamic model by a virtual buoy sensitive to the average current in the upper 30 m layer. No diffusion was considered. Individuals from the egg to the juvenile stages were considered to be transported passively at each time step by the average current in the 30 m surface layer.
Virtual buoys, marking unit water masses, were released on a 10 km x 10 km grid south of 47° N every week during the hatching period of the sampled juveniles and larvae (*i.e*. May to August). The buoy trajectories were stopped on the individuals sampling dates. One trajectory was selected for each individual as its most probable drift trajectory. It was defined as the trajectory beginning on its hatching week and ending at the nearest distance of its sampling location on the sampling date (Allain *et al*., 2003).

2.3. Association of physical and biological data along individual trajectories

Physical variables were estimated at each time step along the trajectories in the hydrodynamic model: temperature, salinity, bathymetry, stratification indices (potential energy deficit and mixed layer depth) and turbulence indices (vertical eddy diffusivity and turbulent kinetic energy dissipation rate). Indices definitions are detailed in the appendix. The physical history (i.e., the time series of the physical variables) recorded along each trajectory was considered to be the environment encountered by each individual. An illustration is given on Figure 3.
These variables were used to derive physical indices representative of the local habitat of larvae and juveniles: average values of the variables over the upper 30 m were calculated, except for stratification

indices which were estimated by definition from surface to bottom (or to 200 m if bathymetry was higher than this limit). Then, as growth was measured every 5 otolith increments, the mean values of the physical indices over 5-day periods were calculated (maximum and minimum values were also calculated for the highly-variable turbulence indices).
The biological and physical data were then stored in a data file containing the values of growth rate, age and physical indices (in columns) estimated for each 5-day period for each individual (in lines). To account for a possible lag between a variation in the physical environment and its effect on growth (Gutierrez and Morales-Nin, 1986 ; Folkvord *et al*., 1997), the physical indices corresponding to one or two 5-day time steps prior to growth rate were also considered.

2.4. Growth model

The growth model concerned the first 100 days post-hatch, a “critical period” when the main (and the most variable) part of mortality is thought to occur in anchovy (Peterman *et al*., 1988). Generalized Additive Models (GAM: Hastie and Tibshirani, 1990) were used to analyse the relationships between growth rate and the physical indices. As growth rate distribution was close to log-normal (Beyer and Laurence, 1981) and variance slightly increased with mean for the younger ages, a log-transformation of growth rate was used in order to stabilize the variance (Hastie et Tibshirani, 1990; Draper et Smith, 1998) and normalise the error distribution.
The general formulation of the model was then :

$$\ln(G_j)=\sum_i T_i(X_i(j))+\varepsilon(j)$$

with G_j : growth rate for the *j*-th observation, X_i : covariates (age and physical variables), T_i : smoothing functions, ε : normally-distributed random error.
A ‘full model’ was first build which included all covariates as linear terms or as spline smoothers with 3 degrees of freedom. The covariate terms were then sorted according to their F-test statistical significance. A standard forward stepwise procedure was then used (S-Plus function step.gam: Venables and Ripley, 2002) to select the most accurate and parsimonious subset of covariates based on the minimization of the Akaike Information Criteria (Hastie and Tibshirani, 1990, chap. 6). Normality in the residuals and their independence to the response were examined. Sensitivity of model selection and prediction to particular data was analyzed by iterating model selection on randomly selected subsets of the data and comparing model prediction to the remaining data (see Discussion).

2.5. Survival model

The relation between growth and survival was investigated using the otolith growth data collected during the surveys mentioned above. Larvae and juveniles with the same spatio-temporal origin were selected and assumed to belong to the same sub-cohorts. The otolith growth rates among the reconstructed sub-cohorts were then compared. The survived juveniles showed faster growth rates during their larval period than the pool of larvae they were estimated to originate from, which supported the idea of growth-selective survival (Allain *et al*., 2003). The survival model was based on that result. It was applied to the same period as the growth model: the first 100 days post-hatch.
A method for modelling growth-selective mortality under the general “bigger is better” hypothesis (Houde, 1987) had been proposed (Hinckley *et al*., 1996; Werner *et al*., 1996), which consisted in setting for each age a minimum size, weight or growth rate considered to be lethal. In the present study the minimal growth rates observed for each age among the survived juveniles were considered as a proxy of these mortality threshold values. The survival model estimated a survival probability based on the statistical properties of the growth model. First, the minimal log growth rate at age observed among the sampled juveniles older than 100 days post-hatch (35 individuals) was considered as the mortality threshold at age (Fig. 4). Then at each time step (*i.e*. age) along a drift trajectory, larval mean growth was estimated with the growth model as a response to the physical parameters. The probability for growth to be higher than the mortality threshold was estimated from the gaussian distribution of the residuals in the growth model. The survival probability *Ps* was thus defined for each individual *i* between age *j-5* and age *j* (in days) as the probability that its growth rate *G* was higher than the mortality threshold *m* defined for this age :

$$Ps_{j-5,\,j}(i,j) = P(G(i,j) > m(j))$$

Along each trajectory, an overall survival probability was defined for each individual *i* as the product of the survival probabilities over its first 100 days post-hatch:

$$Ps_{1,100}(i,j) = \prod_{j=1}^{100} P(G(i,j) > m(j))$$

3. Spawning model

Anchovy spawning in the Bay of Biscay displays a spatio-temporal distribution described by Motos *et al*. (1996). Spawning occurs from April to August (peak in June) and expands progressively from the south-eastern part of the Bay of Biscay towards the north and west. The spatio-temporal process of spawning is not currently monitored and its inter-annual variability is also not well known. We therefore used available data and knowledge to develop a spatio-temporal spawning index that reflected the average annual spatio-temporal spawning process from April to August (22 weeks).
Fish stock assessment surveys are performed by AZTI (egg surveys) and IFREMER (acoustic surveys) close to peak spawning time and over the entire spawning area. The spatial distribution was modelled using data from these surveys. Seasonal variation in spawning was modelled using data from repeated ichtyoplankton surveys (other than the fisheries surveys) that focused on particular spawning grounds but that did not cover the entire area. The interaction between space and time was modelled based on the background knowledge in Motos et al. (1996).
Data from egg surveys performed in 1999 by AZTI (using vertical 'pairovet' hauls) and in 2000, 2001 and 2002 by IFREMER (using Continuous Underwater Fish Egg Sampler) were used to estimate an average egg distibution close to peak spawning time. The spawning area was divided into a grid of 201 squares with a mesh size of 14 nautical miles. In each square *s* and year *y*, the mean egg density $z_{s,y}$ was estimated by the simple average of the data standing in the square. A spatial index $I_{spatial}(s)$ was estimated in each square *s* by taking the proportion of the eggs observed in *s* relative to the total egg observed in all years (1999-2002):

$$I_{spatial}(s) = \sum_{y} z_{s,y} / \sum_{y} \sum_{s} z_{s,y}$$

Then an ogival index was defined for each square and week, derived from the egg densities observed during monthly surveys performed from April to July 1999 on a major spawning ground of anchovy off Gironde estuary (Fig. 2). A gaussian spawning ogive (Fig. 5) was adjusted to the seasonal evolution of the survey average egg density and the ogive peak was standardised to unity. This ogive was attributed to the part of the grid corresponding to 'Gironde' spawning area (Fig. 5). The other spawning areas were attributed the same 'Gironde' ogive but with a lag in time of –2 to +4 weeks (Fig. 5) so as to reproduce the space-time spawning dynamics. Finally, the space-time spawning index *Is* was defined for each square *s* of the grid and for each week *t* from April to August as the product of the spatial and ogival indices relative to this square and week:
$Is(s,t) = I_{spatial}(s) \cdot I_{ogival}(s,t)$
The spatial index thus scaled the peaks of the different spawning ogives considered. The spawning index *Is* was a relative index, giving the percentage of annually spawned eggs that was spawned in each area at each time.

3.1. Simulation of transport, growth and survival

The growth and survival models were run along thousands of virtual buoy trajectories supposed to be indicative of the real trajectories of billions of larvae and juveniles over a whole season. The number of trajectories tracked resulted from a compromise between model precision and computational time. For each year of simulation, virtual buoys were released each week from April to August (22 weeks) from the spawning model grid (201 points) and tracked for 105 days in the hydrodynamic model: 5 days corresponding to average egg and vitelline stages duration (Ré, 1996) and 100 days for larval and juvenile stages. As in most individual-based models (DeAngelis et Gross 1992), only a limited number of individuals could be simulated: 4422 per year in our case, *i.e.* 88440 biophysical simulations (4422 trajectories x 20 5-day periods). Each virtual buoy could be considered as representative of a subcohort of individuals, which is coherent with the 'average individual' formulation of the transport

model. Along each trajectory, the growth rate was estimated every 5 days from the physical environment encountered using the growth model (S-Plus function predict.gam). The survival rate in the subcohort (equivalent to survival probability at the individual scale) was then deduced from the growth rate for every 5-day period. Finally, the overall survival rate *Sr* of a given subcohort *k* was defined as the product of the survival rates over its first 100 days post-hatch:

$$Sr\,(k) = \prod_{j=1}^{100} P(G\,(k,j) > m\,(j))$$

Simulations were performed for the years 1997, 1998 and 1999, years for which wind data from Météo-France ARPEGE model were available.

3.2. Integration and recruitment prediction

All the trajectories were not equivalent: for example, virtual buoys released at peak spawning time represented higher numbers of individuals. The survival index *Si* for a given sub-cohort *k* was then defined as the product of the spawning index *Is* corresponding to the space-time origin of its trajectory by the survival rate *Sr* estimated along its trajectory:

$$Si\,(k) = Is\,(k) \,.\, Sr\,(k)$$

An integrated survival index *S* for a given year *n* was then the sum of the survival indices of all the sub-cohorts over an entire season, divided by the sum of the corresponding spawning indices:

$$S\,(n) = \sum_{k=1}^{4422} Si\,(k) \,/\, \sum_{k=1}^{4422} Is\,(k)$$

This annual survival index corresponded for a given year to a prediction of the mean survival rate during larval and juvenile stages. The spawning index *Is* being relative, the survival index *S* measured survival irrespective of the total number of eggs spawned. The survival index *S* constituted a recruitment index, as larval and juvenile stages corresponded to the “critical period” where the main and the most variable part of mortality was thought to occur. The hindcast predictive capacity of this index was tested on a series of simulated years by comparing its variations with the recruitment assessments performed by the ICES Working Group on Sardine, Anchovy, Mackerel and Horse Mackerel. The values of the index *S* (larval and juvenile survival during year *n*) were compared to the assessment of abundance at age 1 on 1 January of year *n+1.* A proportionality coefficient *K* was estimated by simple linear regression ($R\,(n+1) \approx K\,.S\,(n)$), allowing to convert the survival index expressed in percent into numbers of recruited fish.

4. RESULTS

4.1. Growth and environment along drift trajectories

The larvae and juveniles collected were 5 to 135 days old after hatching. Otolith growth varied in space and time depending on larvae birth date and drift trajectory (Allain *et al*., 2003). Growth rate increased until an age of about 40-50 days then stabilized and progressively decreased (Fig. 6). The reconstructed drift trajectories showed a general pattern with transport directed towards the South, the South-West and the open sea (Allain *et al*., 2003). The latter trajectories exhibited a common seasonal evolution: an increase in temperature and stratification and a decrease in salinity and turbulence.
The covariates selected to best fit the growth model were: age, temperature and stratification index. This 3-covariate model explained more than 86 percent of the total deviance (Fig. 7). The response of growth to stratification was dome-shaped but that to temperature showed no optimum (Fig. 7). The model residuals showed neither major bias nor obvious pattern (Fig. 8) and the normality and heteroscedasticity assumptions were respected.

4.2. Simulation of spawning, transport, growth and survival

The results of the spawning model are illustrated on Fig. 5. Spawning mainly concentrated in two areas: off Gironde and in the Capbreton canyon region. Spawning reached a peak in June, after which it moved towards the North. An example of transport, growth and survival simulation for a single subcohort is illustrated on Fig. 9.
The growth and survival model was fitted on field larvae and juvenile data collected in 1999. For that year the simulated distribution of the survivors agreed with the distribution of the juvenile anchovy catches by the Spanish Basque tuna live bait fishery (Allain *et al.*, 2001b), which suggested a general validity of the transport and survival models at the scale of the season.
The survival indices at the end of the trajectories (100 days post-hatch) of all the sub-cohorts for the years 1997-1999 are illustrated on Fig. 10. The spatial patterns suggested a strong influence of transport (*i.e.* environment encountered along the drift trajectories) on survival.

4.3. Recruitment prediction

The values of the recruitment index for years 1997, 1998 and 1999 are shown on Fig. 11. The recruitment variations predicted by the biophysical simulations (Fig. 11) were close to the variations of recruitment estimates performed by ICES (R^2>0.9). The recruitment index resulting from biophysical simulations agreed better to the ICES recruitment series for the three years analysed than the former correlation index (Allain *et al.*, 2001), suggesting potential improvement in recruitment prediction.

5. DISCUSSION

The methodology used in building the biophysical model required (a) physical data from hydrodynamic model simulations and (b) biological data from classic surveys at sea, hence could be applied to other regions and populations. The modelling approach was driven by biological field data and also simplified the drift processes. The advantage was a direct calibration of the biological model. Its drawback may be a dependence on particular data jeopardizing reliable prediction. These aspects are now discussed.

5.1. Transport modelling

In recent studies (Werner *et al*. 1996, Hinckley *et al*. 1996, Mullon *et al*. 2003), fish larvae were modelled as particles evolving in 3D current fields of hydrodynamic models, which moved according to passive advection and diffusion processes. In these studies it was necessary to impose an active vertical behaviour to the particles so that a realistic proportion of these reached the known nursery areas. This behaviour consisted in vertical daily migrations maintaining the individuals within a particular depth range, which could be determined so as to maximize transport success. A different approach was followed in this study for a number of reasons. The anchovy nursery areas extend over large parts of the Bay of Biscay, which made the notion of transport success difficult to define *a priori*. The depth range for transport was supposed to correspond to the habitat (upper layer) where anchovy larvae and juveniles have been observed (Petitgas et al., 2004). The consideration of diffusion in the back-tracking procedure implied very high computational time and cost. Besides, recent tracking experiments of real buoys on the French shelf of the Bay of Biscay (Lazure, unpublished data) showed the dominance of advective (deterministic) movement due to tides and winds over diffusive (turbulent) movement. The hypothesis made in this study was that individual transport could be approximated by passive transport according to the average advective current within the depth range of the larvae/juvenile habitat. This simple transport model was able to reproduce the general transport scheme of anchovy larvae and juveniles from spawning to nursery areas in the Bay of Biscay (Allain *et al*. 2001b). More validation studies would be helpful, such as comparisons with real buoy trajectories and with transport simulations including diffusion.

5.2. Growth model validation

As additional individuals were not available, the following resampling technique was used for the validation of the growth model. (a) A proportion (0.6) of the whole sample of N individuals was randomly selected, (b) a growth model was selected using the p selected individuals only and (c) the growth rates predicted by this model were compared to the observed rates for the remaining N-p individuals. The procedure (a, b, c) was repeated a hundred times. The models selected in the validation procedure resulted to be all similar (with age, stratification and temperature as most significant covariates), which suggested a low sensitivity of the model structure to the data. The comparison between predicted and observed individual growth rates (Fig. 12) showed that mean growth rate was well estimated while variance around the mean was slightly underestimated. The sensitivity of the growth model to the association procedure of individuals with trajectories was also examined: individuals were associated with the second and third nearest trajectory when considering to the distance between sampling location and virtual buoy location on the date of sampling. The growth models build using these different trajectories also resulted to be very similar to the original one (same significant covariates), due to the similar evolution of physical variables recorded along those close trajectories. Indeed, the fields of the growth model covariates simulated by the hydrodynamic model were smooth.

5.3. Growth and environment along drift trajectories

Otolith growth rate in the early life stages was related to age, stratification and temperature. The strong dependence of growth rate on age (Fig. 7) was related to the major morphological transformations during larval and juvenile stages. At the age of 40-50 days post-hatch growth rate reached a maximum corresponding to the onset of metamorphosis (Ré, 1996). The positive influence of temperature on growth in early life stages has been widely observed in both natural environment and rearing experiments (Ricker 1979). The results would indicate a temperature optimum close to 19-20°C. The dome-shaped relationship observed between stratification index and growth rate suggested that moderately stratified waters would be favorable to growth. MacKenzie *et al*. (1994) and Sundby

(1997) observed a dome-shaped relationship between turbulence and larval fish ingestion rates. At a broader scale, Cury and Roy (1989) noticed a dome-shaped relationship between wind intensity and recruitment of small pelagic fish in upwelling systems. Though general ecological knowledge supported the dome-shaped relationship between growth and water column stratification, the precise processes underlying the relationship are still hypothetical. Highly stratified (*i.e.* open ocean) waters could be unfavorable to growth because of generally low productivity and low encounter rates with prey. Unstratified (*i.e*. coastal or wind-mixed) waters could be detrimental to food intake by larvae and/or dispersion of plankton aggregates.

5.4. Sensitivity of survival to the growth threshold

The mortality rates over 5-day periods predicted by the survival model decreased strongly with age (Fig. 9), which was coherent with the results of larval mortality studies (Houde, 1987). The sensitivity of the survival model to the mortality threshold values was studied as follows. The simulation corresponding to peak spawning (mid-June release of virtual buoys) was repeated 10 times, with mortality threshold values being each time modified by a certain percentage around their initial value (from –50% to +50%). A 10 % variation in mortality threshold values resulted in a variation of about 5% on the mean survival probability over 5 days, hence in multiplying the mean survival probability at 100 days post-hatch by a factor ranging from 5 to 10 (Fig. 13). The overall survival rates calculated with the biophysical model (Fig. 11) were coherent with that estimated by Peterman *et al*. (1988) for *Engraulis mordax.*

5.5. Recruitment prediction

This study was an attempt to simulate the recruitment process by integrating individual growth and survival over the population distribution in space and time. The biophysical model predicted variations in recruitment compatible with the ICES series in the 3 year period studied. A higher number of years will off course be necessary to fully assess the predictive capacity of the biophysical model. A first limit in the reliability of prediction lies in extrapolation, as models fitted on a limited number of observations are run for simulations over a broader range of parameter values, time and space intervals than that observed. We compared the distributions of the growth model covariates (temperature and stratification along the trajectories) used for model construction with that simulated for prediction (Fig. 14). The comparison revealed no major bias, meaning that prediction was made with environmental parameter values in the range of that observed. Extra individuals (larvae and juveniles) would nevertheless be precious to further validate the growth and survival models by exploring a larger part of the variability of physical-biological interactions. A second limit of the biophysical simulations lies in simplification (which is inherent to modelling). Many elements were absent from the biophysical model presented here: processes related to transport (general circulation and deep slope currents, small-scale eddies, etc.), biological processes not related to the physical variables of the growth model (inter-annual spawning variability, larval prey size, predation, density-dependence, stock demography, etc.). The modeling choices resulted from a compromise between accuracy and precision. Compared to the correlation index (Fig. 11), the 'biophysical' recruitment index required more computations but was likely to be more reliable because it integrated fine-scale processes and transport from individual to population scales. This study constituted a further step towards the objective of operational recruitment prediction and integration of environmental variability into fisheries management.

ACKNOWLEDGEMENTS

This study was part of a PhD work which was co-financed by IFREMER, Région Pays de la Loire and Comité National des Pêches Maritimes (Commission de l'anchois et de la sardine). It contributed to the IFREMER project FOREVAR (environmental forcing and stock variability) affiliated to GLOBEC. We would like to thank A. Uriarte (AZTI) for making some egg data available and C. Roy (IRD) and P. Gros (IFREMER) for their constructive comments.

REFERENCES

Allain G., Petitgas P., Lazure P. and Grellier P. (2001) The influence of mesoscale ocean processes on anchovy (*Engraulis encrasicolus*) recruitment in the Bay of Biscay estimated with a three-dimensional hydrodynamic model. *Fish. Oceanogr.* 10: 151-163.

Allain G., Petitgas P., Lazure P. and Grellier P. (2001b) The transport of anchovy larvae and juveniles across the Bay of Biscay studied using otolith increments and a 3D hydrodynamic model. ICES CM 2001/W:01.

Allain G., Petitgas P., Grellier P. and Lazure P. (2003) The selection process from larval to juvenile stages of anchovy in the Bay of Biscay investigated by Langrangian simulations and comparative otolith growth. *Fish. Oceanogr.* 12(4/5): 407-418.

Bartsch J. and Coombs S.H. (2001) An individual-based growth and transport model of the early life-history stages of mackerel (Scomber scombrus) in the eastern North Atlantic. *Ecol.I Mod.* 138: 127-141.

Bartsch J. and Coombs S.H. (2004) An individual-based model of the early life history of mackerel (Scomber scombrus) in the eastern North Atlantic, simulating transport, growth and mortality. *Fish. Oceanogr.* 13: 365-379.

Beyer J.E. and Laurence G.C. (1981) Aspects of stochasticity in modelling growth and survival of clupeoid fish larvae. *Rapp. P.-v. Cons. Int. Explor. Mer.* 178: 17-23.

Borja A., Uriarte A., Valencia V., Motos L., and Uriarte A. (1996) Relationships between anchovy (*Engraulis encrasicolus*) recruitment and the environment in the Bay of Biscay. *Sci. Mar.* 60 (Suppl. 2): 179-192.

Campana S.E. and Jones C.M. (1992) Analysis of otolith microstructure data. *Can. Spec. Publ. Fish. Aquat. Sci*. 117: 73-100.

Cermeño P., Uriarte A., de Murguía A.M. and Morales-Nin B. (2003) Validation of daily increment formation in otoliths of juvenile and adult European anchovy. *J. Fish Biol.* 62: 679-691.

Chambers R. and Trippel E. (1997) *Early Life History and recruitment in fish populations.* Chapman and Hall, London, 596p.

Cury P. and Roy C. (1989) Optimal environmental window and pelagic fish recruitment success in upwelling areas. *Can. J. Fish. Aquat. Sci*. 46: 670-680.

De Young B., Heath M., Werner F., Chai F., Megrey B. and Monfray P. (2004) Challenges of modeling ocean basin ecosystems. *Science* 304: 1463-1466.

DeAngelis D.L. and Gross L.J. (1992) *Individual-based models and approaches in ecology. Populations, communities and ecosystems*. Chapman & Hall, New York, 525p.

Draper N.R. and Smith H. (1998) *Applied Regression Analysis*. Wiley & Sons, New York, 706p.

Folkvord A., Rukan K., Johannessen A. and Moksness E. (1997) Early life history of herring larvae in contrasting feeding environments determined by otolith microstructure analysis. *J.Fish.Biol.* 51(A): 135-154.

Garcia A. and Palomera I. (1996) Anchovy early life history and its relation to its surrounding environment in the Western Mediterranean basin. *Sci. Mar*. 60 (Supl.2): 155-166.

Garcia A., Cortes D. and Ramirez T. (1998) Daily larval growth and RNA and DNA content of the NW Mediterranean anchovy Engraulis encrasicolus and their relations to the environment*. Mar. Ecol. Prog. Ser.* 166: 237-245*.*

Gutierrez E. and Morales-Nin B. (1986) Time series analysis of daily growth in Dicentrarchus labrax L. otoliths. *J. Expl. Mar. Biol. Ecol*. 103: 163-179

Hastie T.J. and Tibshirani R.J. (1990) *Generalized Additive Models*. Chapman & Hall, London, 335p.

Heath M. and Gallego A. (1997) From the biology of the individual to the dynamics of the population: bridging the gap in fish early life studies. *J. Fish Biol.* 51 (Suppl. A): 1-29.

Hermann A.J., Hinckley S., Megrey B.A. and Napp J.M. (2001) Applied and theoretical considerations for constructing spatially explicit individual-based models of marine larval fish that include multiple trophic levels. *ICES J. Mar. Sci*. 58: 1030-1041.

Hinckley S., Hermann A. and Megrey B. (1996) Development of a spatially-eplicit, individual-based model of marine fish early life history. *Mar. Ecol. Prog. Ser*. 139: 47-68.

Hinckley S., Hermann A. and Megrey B. (2000) An evaluation of the utility of spatially explicit biophysical models in recruitment studies: the FOCI example. ICES CM 2000/N:12

Houde E.D. (1987) Fish early life dynamics and recruitment variability. *Am. Fish. Soc. Symp.* 2: 17-29.

ICES (2004) Report of the Working Group on the Assessment of Mackerel Horse mackerel Sardine and Anchovy. ICES CM 2004/ACFM:07.

Jégou A.M., Dumas F. and Lazure P. (2001) Modelling the Adour plume with a 3D hydrodynamic model. In : *Actes du VIIe Colloq. Intern. Océan. Golfe de Gascogne*. J. d'Elbée and P.Prouzet (eds). Editions Ifremer, Actes Colloq. 31: 49-54.

Larkin P. (1996) Concepts and issues in marine ecosystem management. *Rev. Fish Biol. Fish.* 6: 139-164.

Lazure P. and Jégou A.-M. (1998) 3D modelling of seasonal evolution of Loire and Gironde plumes on Biscay Bay continentel shelf. *Oceanologica Acta* 21: 165-177.

Longhurst A. (1998) Cod : perhaps if we all stood back a bit. *Fish. Res.* 38: 101-108.

Lynch D., Naimie C. and Werner F. (1996) Comprehensive coastal circulation model with application to Gulf of Maine. *Cont. Shelf Res.* 16: 875-906.

Mackenzie B.R., Miller T.J., Cyr S. and Leggett W.C. (1994) Evidence of a dome-shaped relationship between turbulence and larval fish ingestion rates. *Limnol. Oceanogr*. 39: 1790-99.

Megrey B., Hollowed A., Hare S., Macklin A. and Stabeno P. (1996) Contributions of FOCI research to forecasts of year class strength of walleye pollock in Shelikof Strait, Alaska. *Fish. Oceanogr.* 5 (Suppl.1): 189-203.

Motos L., Uriarte A. and Valencia V. (1996). The spawning environment of the Bay of Biscay anchovy (*Engraulis encrasicolus*, L.). *Sci. Mar.* 60 (Suppl.2): 117-140.

Mullon C., Fréon P., Parada C., Van der Lingen C. and Huggett J. (2003) From particles to individuals : modelling the early stages of anchovy in the southern Benguela. *Fish. Oceanogr*. 12 (4/5): 396-406.

Myers R. (1998) When do environment recruitment relation work? *Rev. Fish Biol. and Fish.* 8: 285-305.

Palomera I., Morales-Nin B. and Lleonart J. (1988) Larval growth of anchovy, *Engraulis encrasicolus*, in the Western Mediterranean Sea. *Mar. Biol*. 99: 283-91.

Palomera I. (1991) Vertical distribution of anchovy larvae *Engraulis encrasicolus* in Western Mediterranean. ICES *CM* 1991/L:31

Peterman R.M., Bradford M.J., Lo N.C. and Methot R.D. (1988) Contribution of early life stages to interannual variability in recruitment of Northern Anchovy. *Can. J. Fish. Aquat. Sci*. 45: 8-16.

Petitgas P., Beillois P., Massé J. and Grellier P. (2004) On the importance of adults in maintaining population habitat occupation of recruits as deduced from observed schooling behaviour of age-0 anchovy in the bay of Biscay. ICES CM 2004/J:13.

Ré P. (1986) Otolith microstructure and the detection of life history events in sardine and anchovy larvae. *Ciênc. Biol. Ecol. Syst.* (Portugal) 6: 9-17

Ré P. (1996) Anchovy spawning in Mira estuary (SW Portugal). *Sci.Mar.* 60 (suppl.2) : 141-153

Ricker W.E. (1979) *Growth rates and models*, p. 677-743. *In*: W.S. Hoar, D.J. Randall and J.R. Brett [ed.] Fish Physiology, Vol VIII., Academic Press, N.Y.

Shepherd J.G., Pope J.G. and Cousens R.D. (1984) Variations in fish stocks and hypotheses concerning their links with climate. *Rapp. P.-v. Réun. Cons. int. Explor. Mer* 185: 255-267.

Uriarte A., Prouzet P. and Villamor B. (1996) Bay of Biscay and Ibero Atlantic anchovy populations and their fisheries. *Sci. Mar.* 60 (Suppl. 2): 237-255.

Sundby S. (1997) Turbulence and ichthyoplankton : influence on vertical distributions and encounter rates. *Sci. Mar.* 61 (Suppl. 1): 159-176.

Venables W. and Ripley B. (2002) *Modern applied statistics with S*. 4th Ed. Springer Verlag, New York, 495p.

Werner F.E., Page F.H., Lynch D.R., Loder J.W., Lough R.G., Perry R.I., Greenberg D.D. and Sinclair M.M. (1996) Influences of mean advection and simple behavior on the distribution of cod and haddock early life stages on Georges Bank. *Fish. Oceanogr*. 2: 43-64.

APPENDIX: Stratification and turbulence indices estimated along the drift trajectories

5.6. Stratification indices

Potential energy deficit Φ (i.e. the stratification index considered in the biophysical growth model) was equal to the energy necessary to homogenise the density in the water column :

$$\Phi = \frac{1}{H+\xi} \int_{-H}^{\xi} \left(\overline{\rho} - \rho_z\right) g \; z \; dz$$

with : $\overline{\rho} = \frac{1}{H+\xi}\int_{-H}^{\xi} \rho_z dz$, ρ_z : density at depth z, and *H* : water depth

Mixed layer depth (h_s) : the water column was considered to be composed of two distinct layers with homogenous densities, a surface layer with height h_s and a bottom layer with height h_b. The state equation $\rho g H = \rho_s g h_s + \rho_b g h_b$ can be used to estimate $h_s = H (\rho-\rho_b) / (\rho_s-\rho_b)$, with H: total water depth, ρ: mean density from surface to bottom, ρ_s: surface density and ρ_b: bottom density being known parameters.

5.7. Turbulence indices

Vertical eddy diffusivity *Kz* from surface to bottom ($m^2 s^{-1}$) represented the mixing effect on the water column induced by wind-driven turbulence : $\tau (z,t) = \rho Kz (z,t) \partial u(z,t)/\partial z$ (τ: vertical shear stress(kg m^2 s^{-1}), ρ: density, u: horizontal component of velocity).

Turbulent kinetic energy dissipation rate ε integrated the dissipation of turbulent kinetic energy over the different scales: $\varepsilon = 2\nu \int_0^{\infty} k^2 E(k) dk$ with ν the kinetic viscosity and $k^2E(k)$ the kinetic energy dissipation spectrum. This variable has been widely used for the study of turbulence effects on fish larvae (e.g., Mackenzie *et al*., 1994; Sundby, 1997).

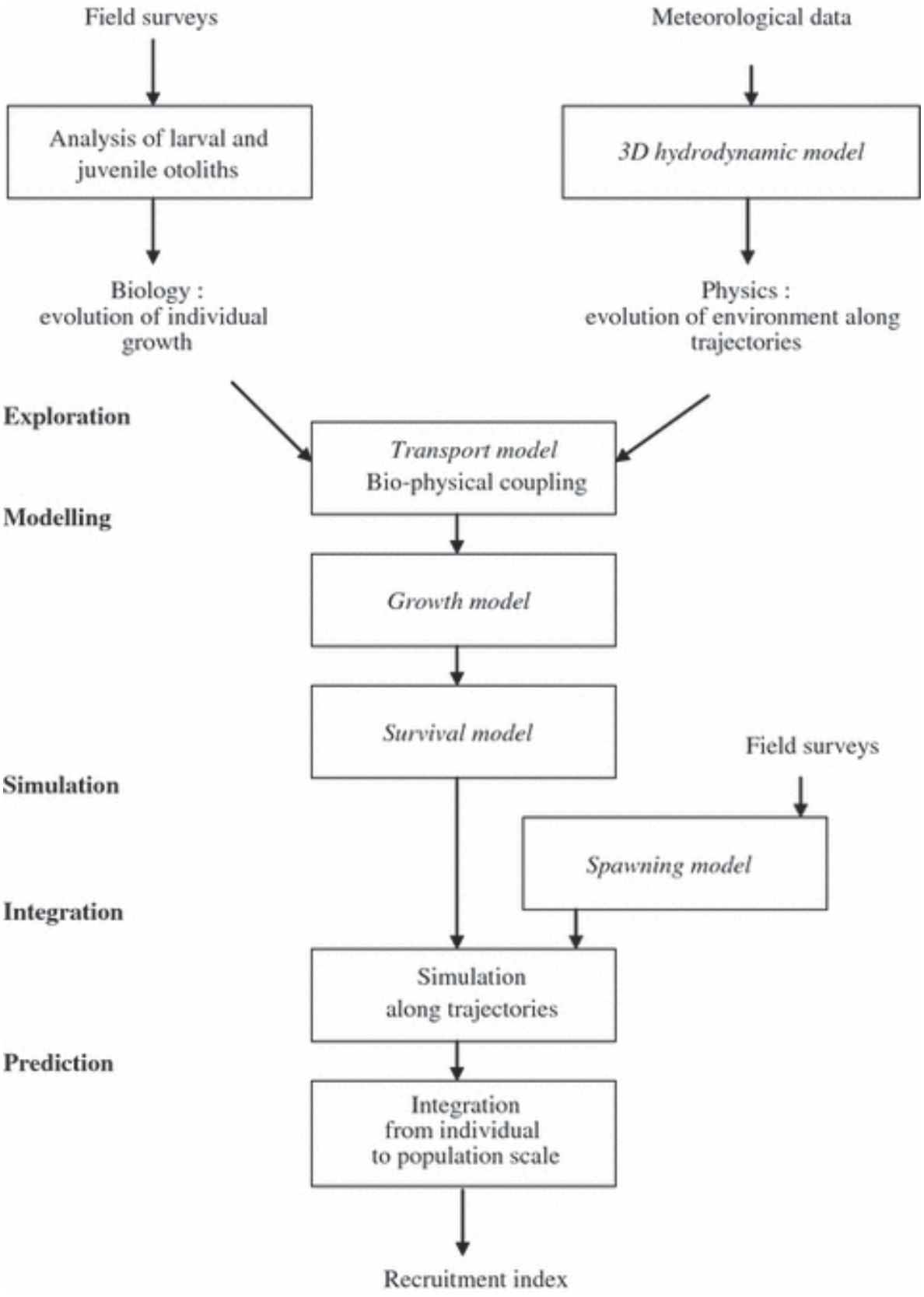

Figure 1: Synthetic description of the successive steps in the approach followed in the paper.

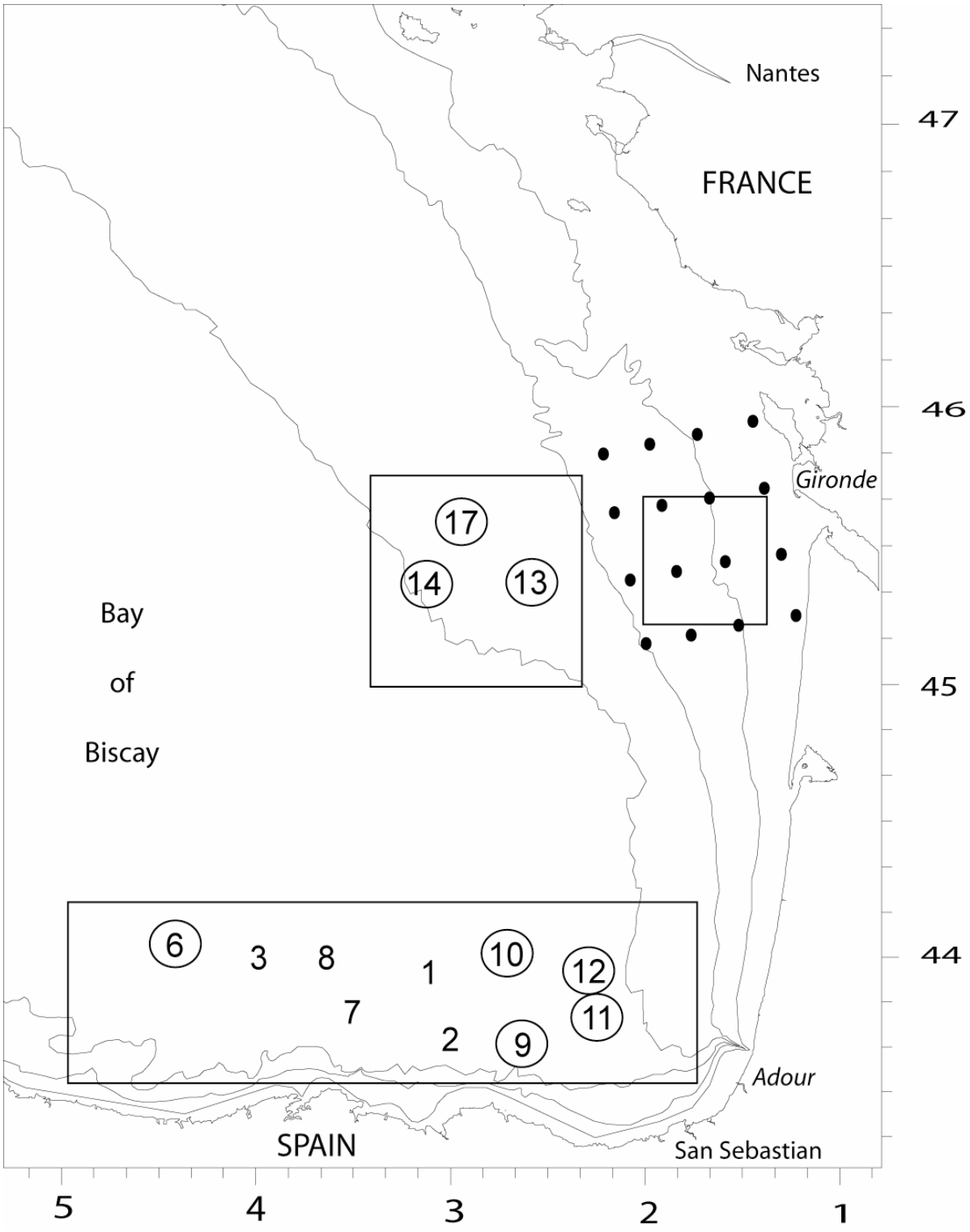

Figure 2: Description of larval and juvenile surveys in 1999. The black dots correspond to the sampling locations of eggs and larvae during monthly surveys from April to July 1999 (PLAGIA repeated surveys of IFREMER). The rectangles represent the areas prospected during a juvenile survey in September1999 (JUVESU survey of IFREMER and AZTI). The numbers correspond to the positions of trawl hauls with anchovy juveniles, the circled numbers to the samples used for otolith analyses.

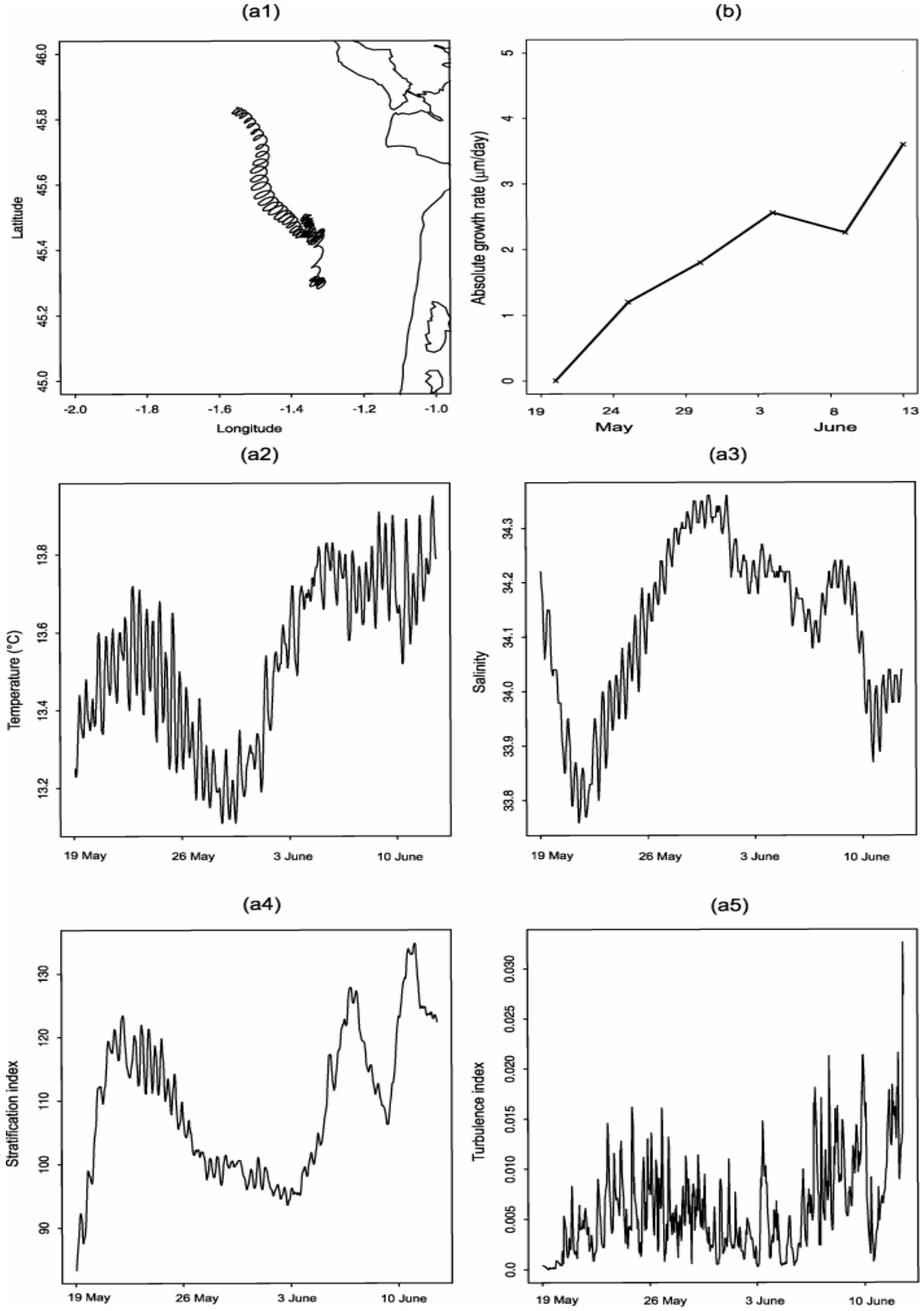

Figure 3: Illustrative example of associated physical and growth histories. (a1-a5): Evolution of the physical environment along the trajectory of a virtual buoy estimated by MARS3D hydrodynamic model. (b): Evolution of otolith growth of a larva collected in June 1998. (a1): Trajectory of the virtual buoy (presumed drift of the larva) from 17 May to 13 June 1998. (a2-a5): Hourly evolution of (a2) temperature, (a3) salinity, (a4) stratification index and (a5) turbulence index, averaged over the 0-30 m layer . (b): Otolith growth rate (µm day^{-1}) by 5-day periods from 17 May to 13 June 1998 .

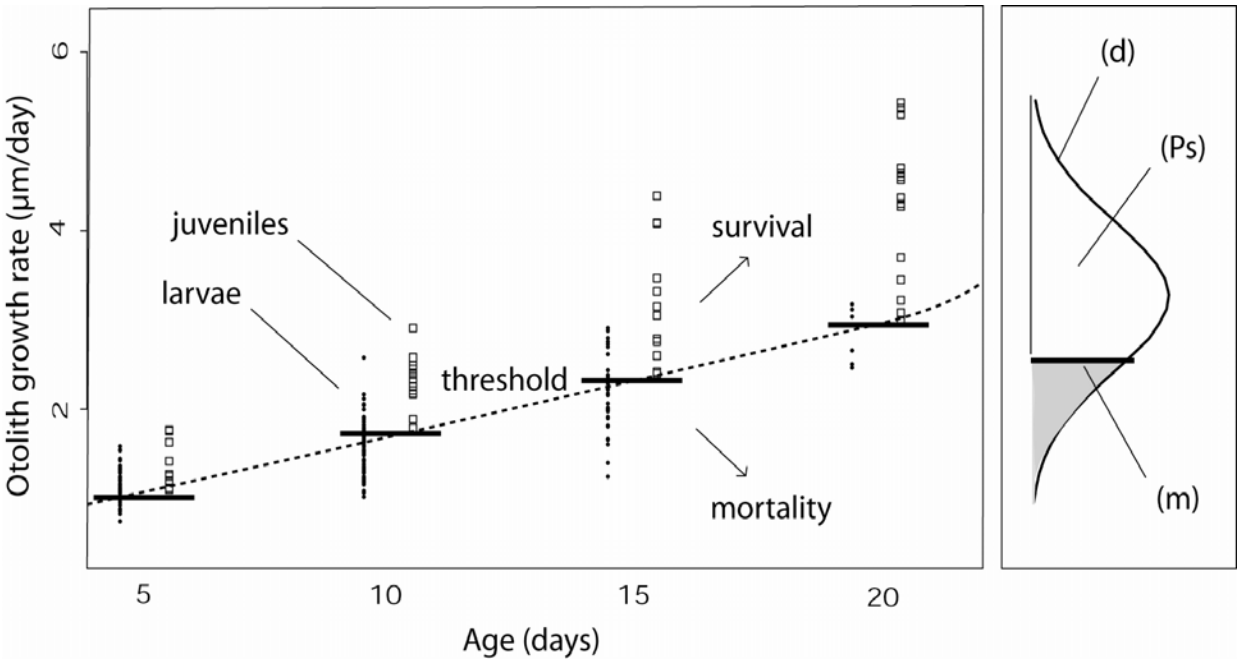

Figure 4: Survival model diagram. Left: the minimal growth rates at age observed among the survived juveniles that were considered as mortality thresholds at age. Right: the probability (1-Ps) for growth at age (in log) to be higher than the mortality threshold at age (m, in log) that was estimated from the gaussian distribution (d) of the residuals of the growth model.

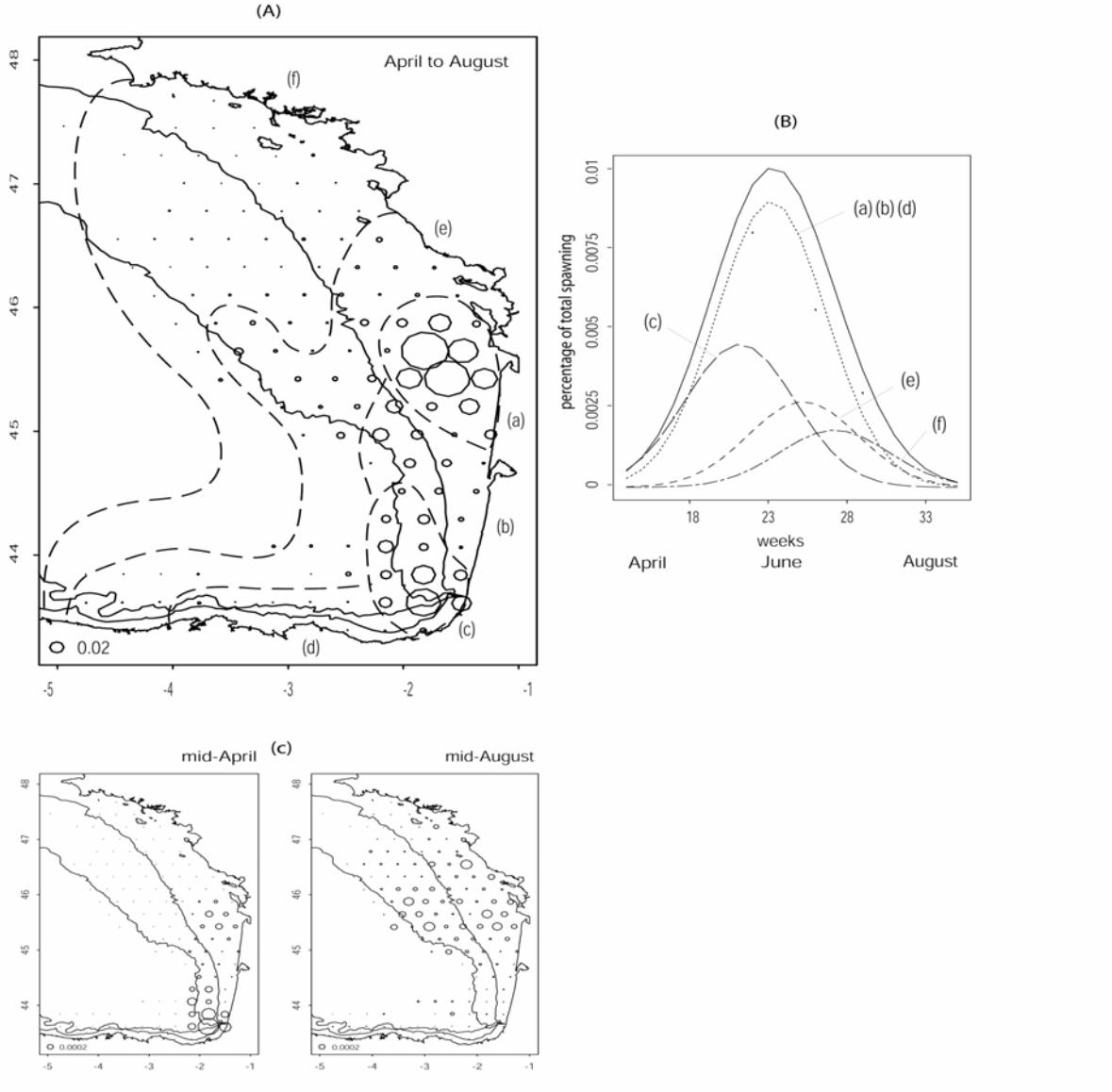

Figure 5: Space-time spawning model.
(A) Spatial distribution of spawning summed over the entire season (April to August). The circle radius at each point of the grid is proportional to the sum of weekly spawning abundance indices in the corresponding area. The circle in the bottom left corner represents 2% of total spawning. The dashed lines correspond to the limits of the spawning areas defined in the model : (a) Gironde (b) Landes (c) Capbreton (d) Cantabrico (e) Rochebonne (f) North.
(B) Temporal distribution of spawning from April to August. The solid curve represents the total ogive, *i.e.* the sum of spawning abundance indices by week over the entire bay. The other curves represent the ogives for each spawning area. The black dots correspond to the relative monthly egg densities observed in the Gironde area in 1999.
(C) Evolution of spawning distribution during the spawning season, as estimated by the spawning model.

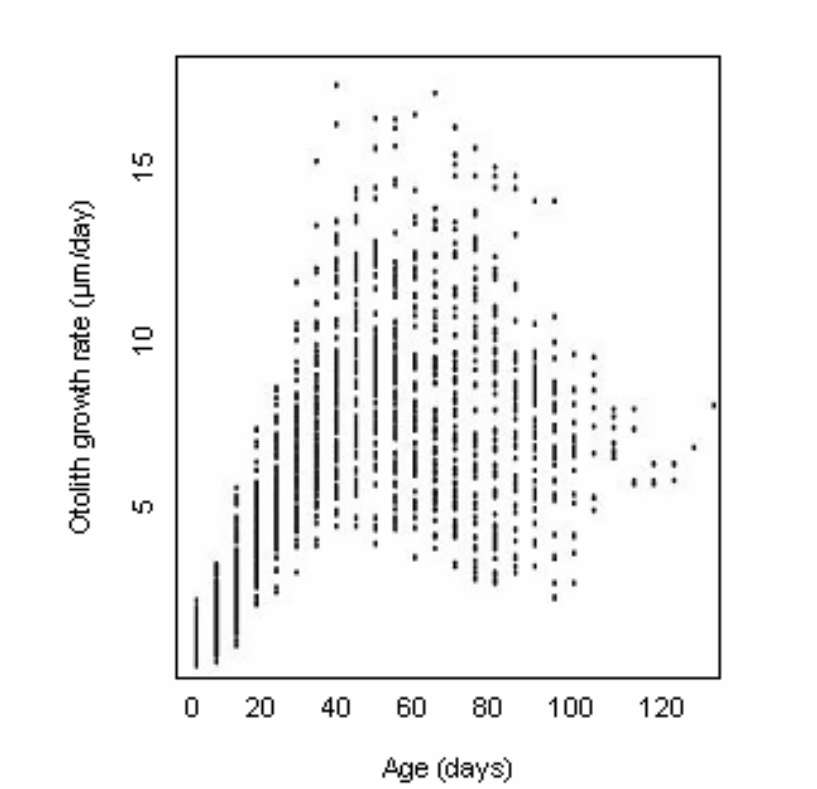

Figure 6: Otolith growth rate (µm day^{-1}) versus age (days) of the anchovy larvae and juveniles collected in 1999 in the Bay of Biscay.

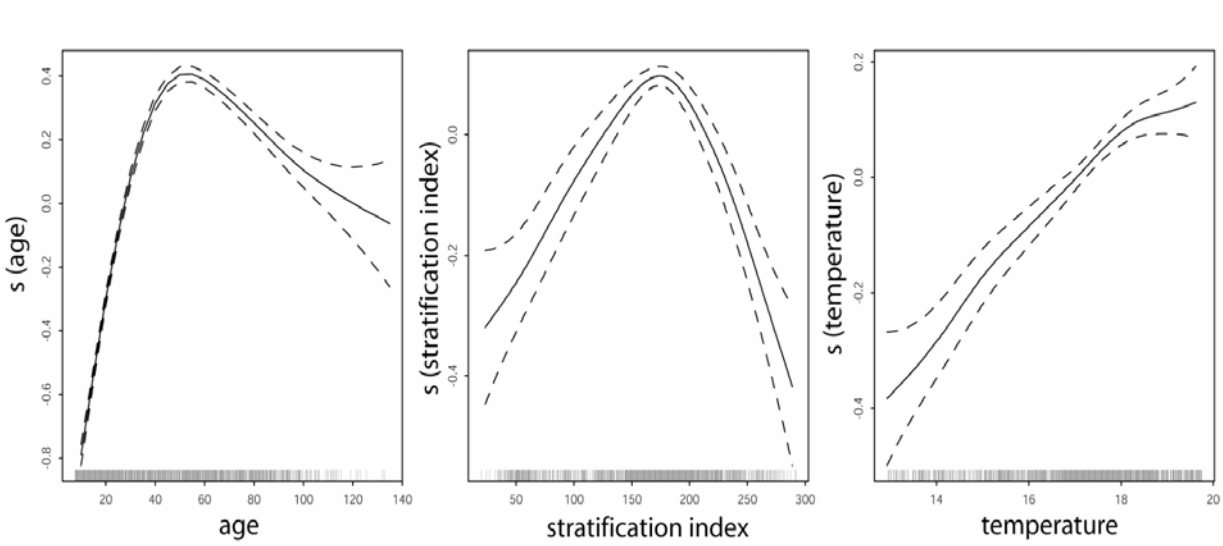

Figure 7: Generalised Additive Model of instantaneous growth as a response to age, water column stratification index and temperature, during the first 100 days post hatch. The curves (solid lines) show the effect of each covariate on the linear predictor of growth. 95% confidence limits around the covariate effects are also shown (dashed lines). Note that the growth response to temperature in the range 12-20°C is not dome-shaped in contrast to the response to age and stratification.

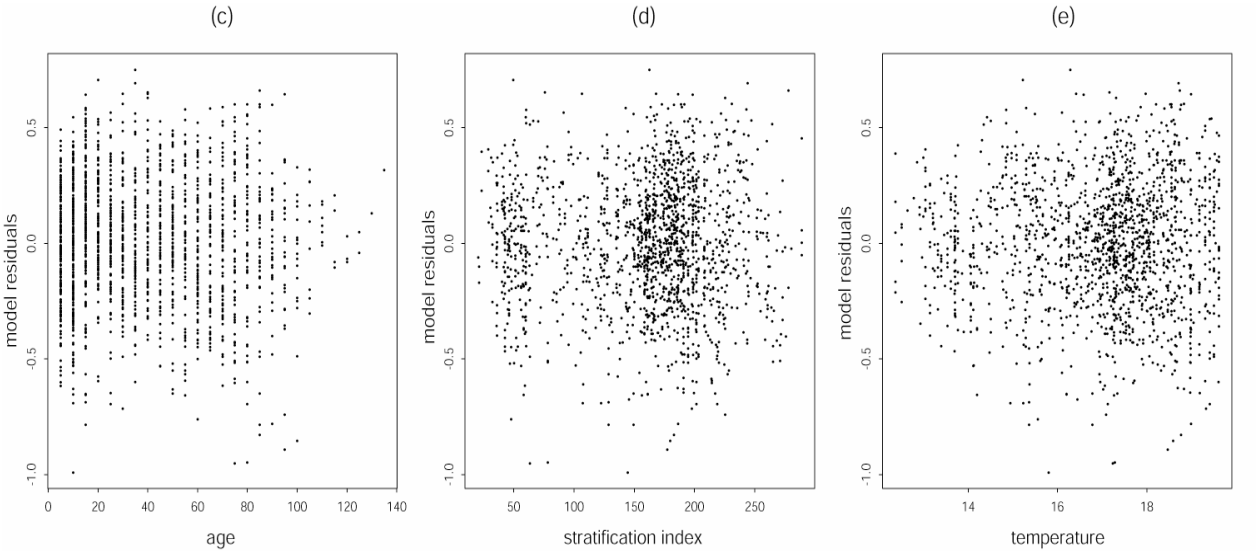

Figure 8: Growth model residuals versus (a) quantiles of standard Normal, (b) fitted values, (c) age, (d) stratification index and (e) temperature.

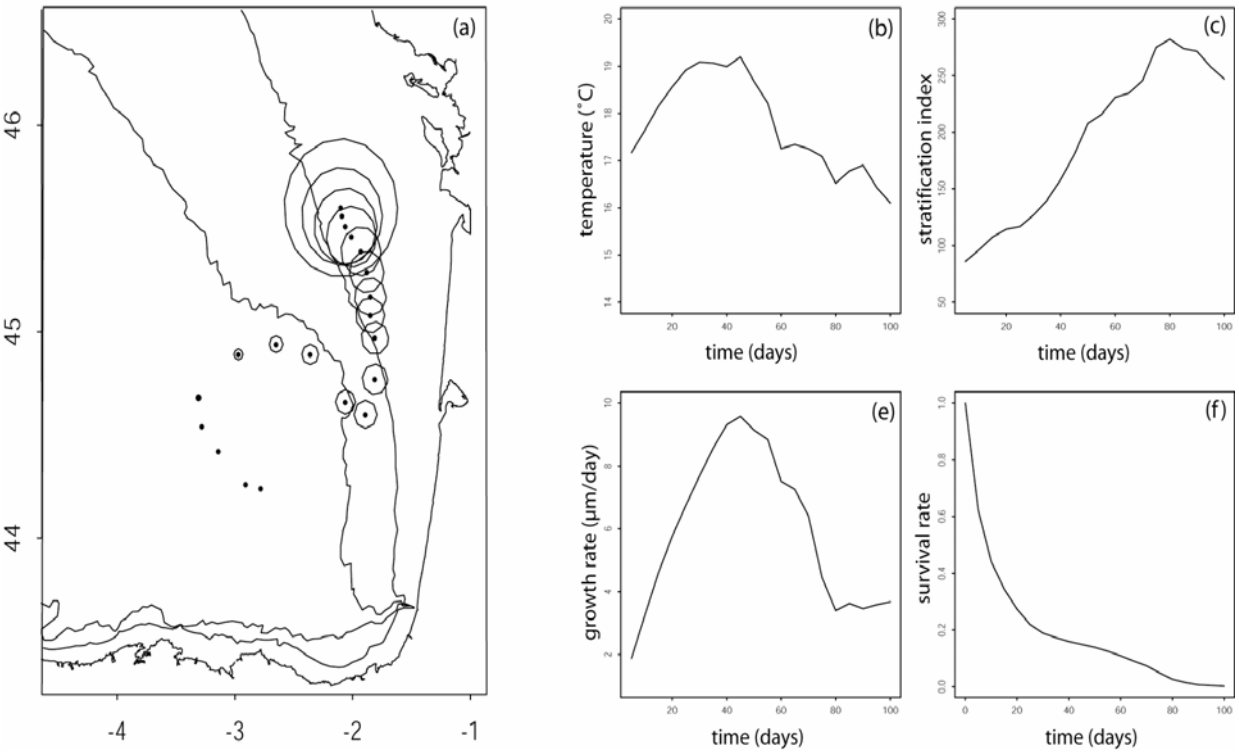

Figure 9: Illustrative example of simulated growth and survival along one trajectory tracked in the hydrodynamic model. (a) : virtual buoy trajectory (points) from its release location (45°30'N, 2°W). (b) and (c): evolution of temperature and stratification index along the trajectory. (e) and (f) : evolution of mean instantaneous growth rate and cumulative survival rate along the trajectory. The circles radius in (a) is proportional to the cumulative survival rate along the trajectory.

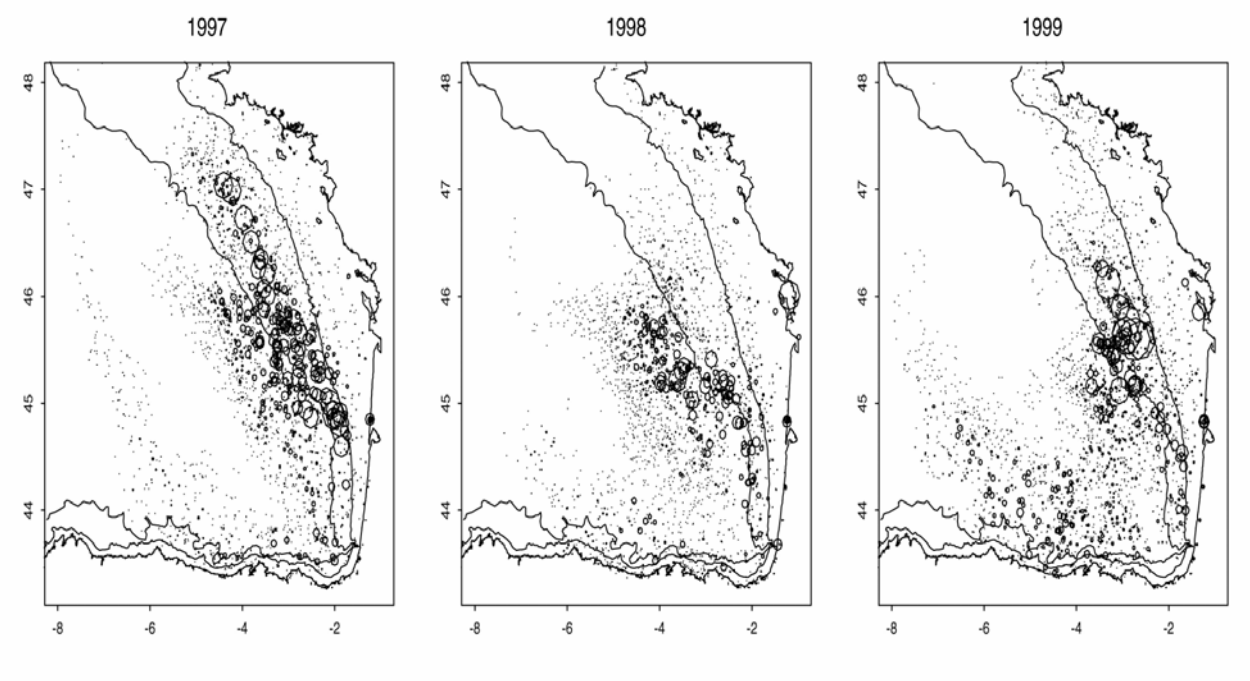

Figure 10: Survival indices at 100 days post hatch of all the sub-cohorts born from April to August for years 1997, 1998 and 1999. The circles positions correspond to the arrival of the drift trajectories, *i.e*. the position of the sub-cohorts at the age of 100 days post hatch. Each circle radius is proportional to the survival probability integrated along the trajectory (simulation result) multiplied by the spawning index at the trajectory origin.

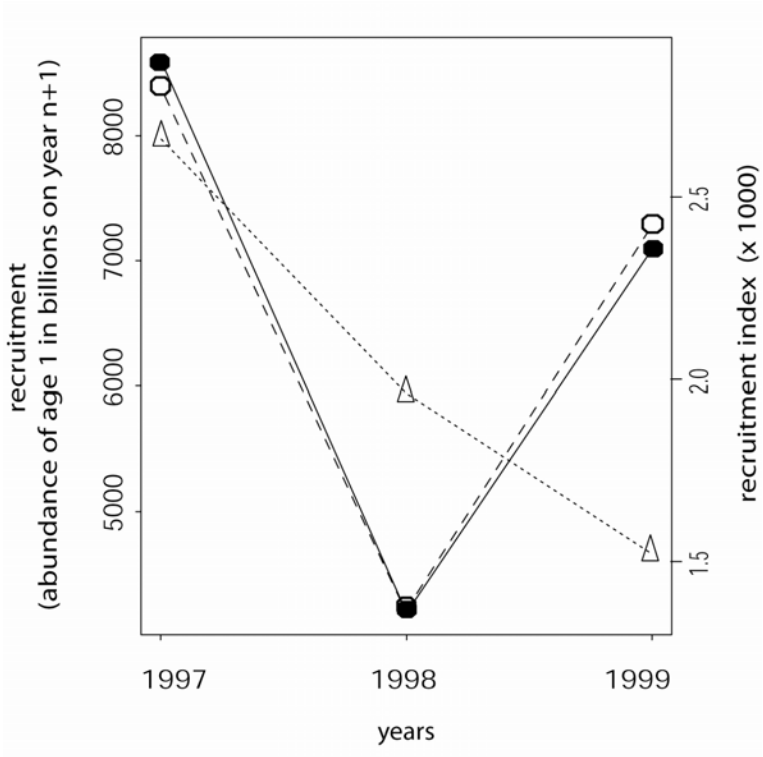

Figure 11: Comparison between the biophysical model recruitment index and other recruitment estimates for the years 1997-1999. Annual recruitment estimations (ICES, 2003) Black dots and solid line: ICES recruitment series (ICES, 2004); white dots and dashed line: biophysical recruitment index; triangles and dotted line: correlation-based recruitment index of Allain *et al*. (2001).

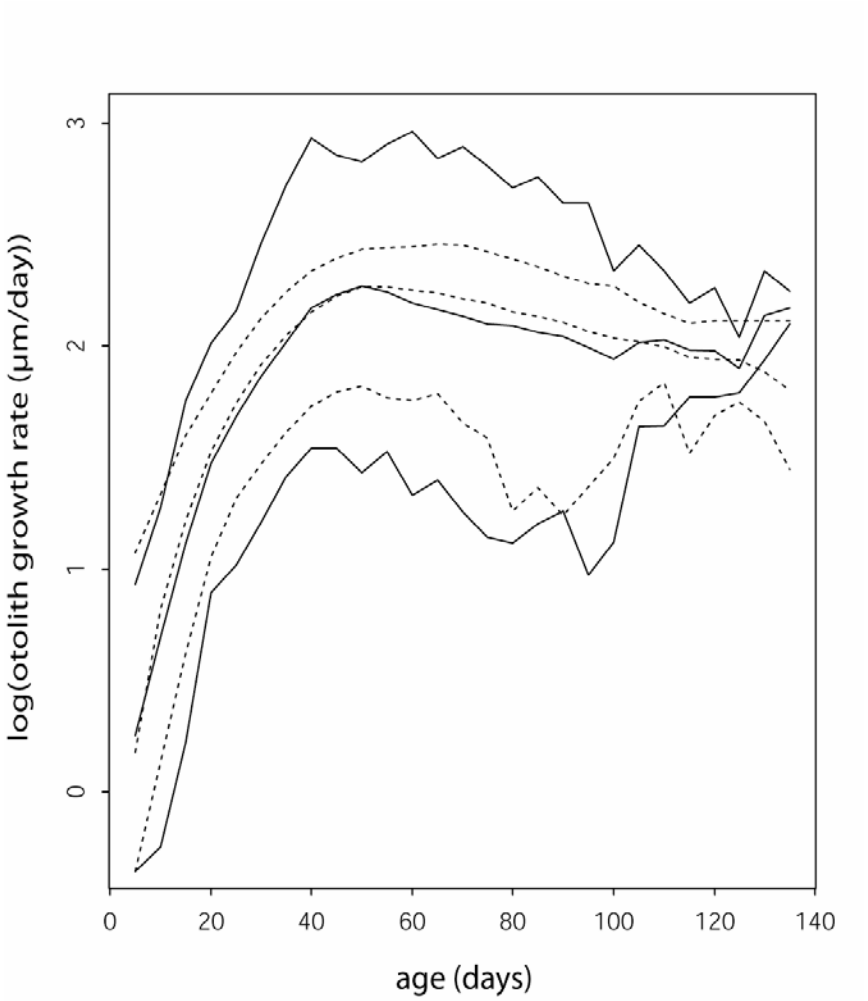

Figure 12: Validation of the growth model. Solid curves correspond to the minimum, mean and maximum growth rates for the validation individuals. Dotted curves correspond to the minimum, mean and maximum growth rates predicted by the growth model.

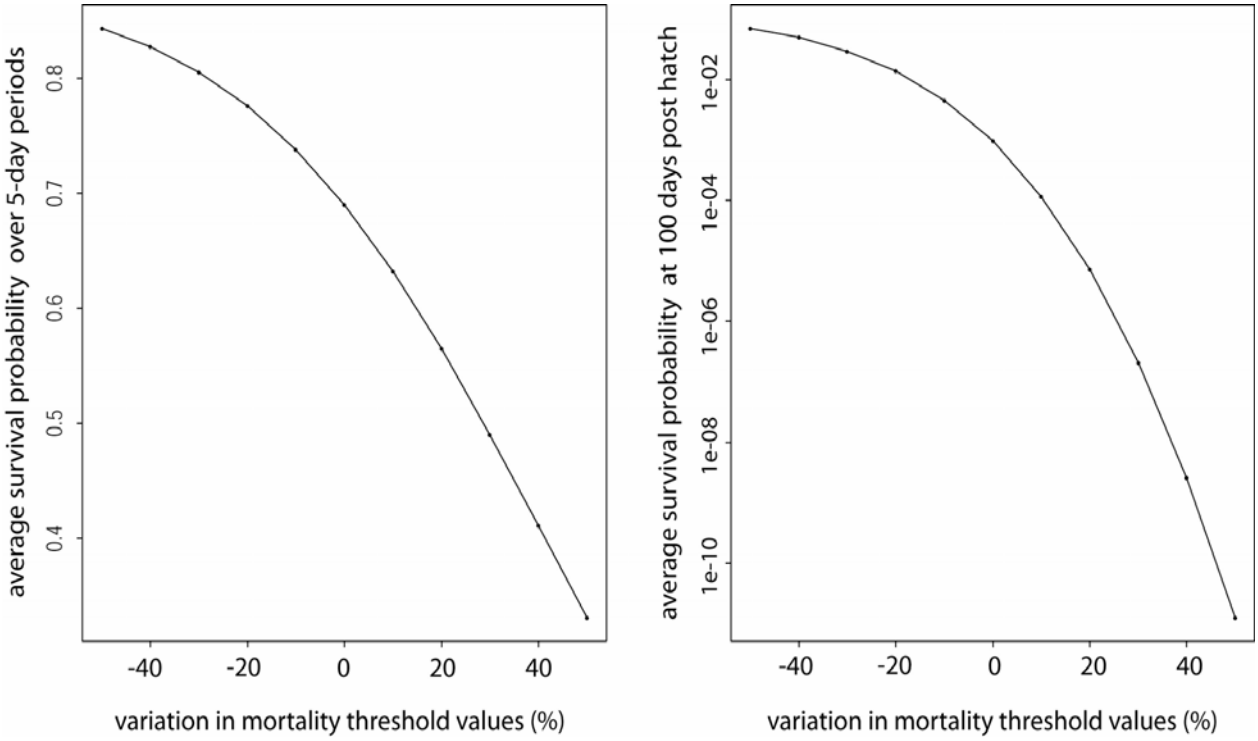

Figure 13: Sensitivity of the survival model to variation in the mortality threshold. Left: influence on the average survival probability over 5-day periods for all the trajectories released. Right: influence on the average survival probability at 100 days post hatch for all the trajectories released.

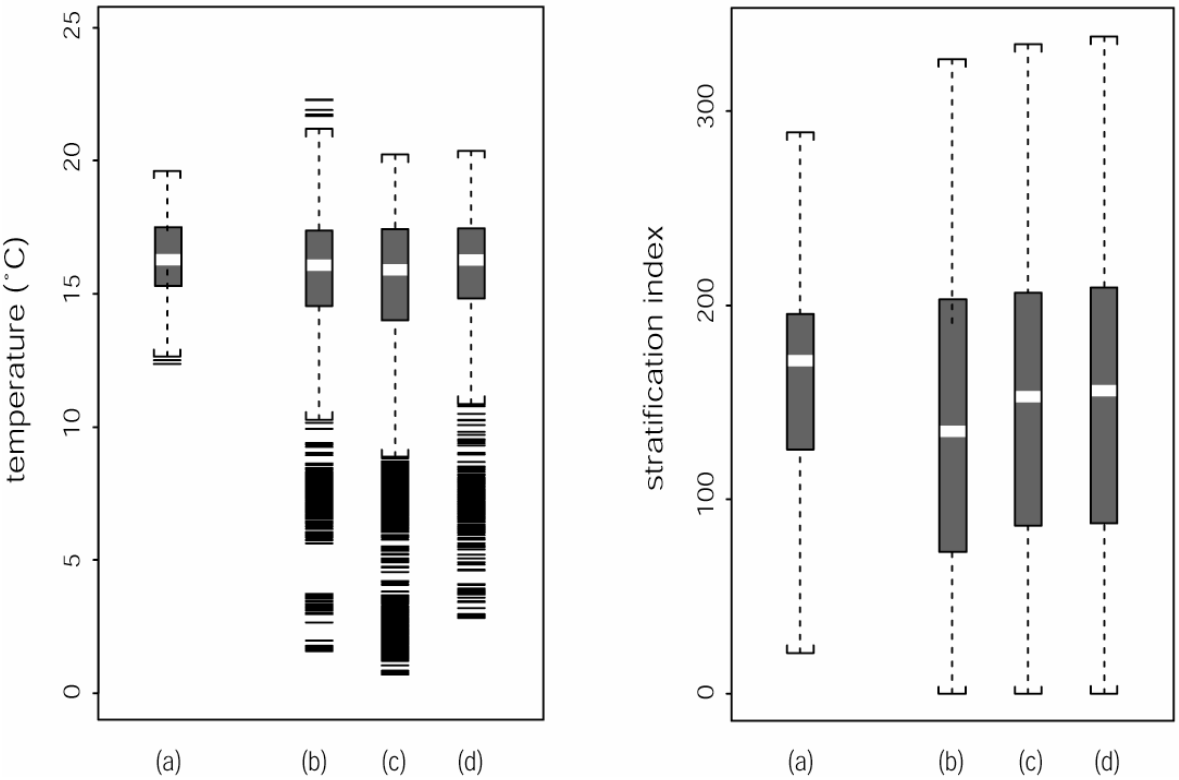

Figure 14: Comparison between the range of covariate values used for fitting the growth model (a) and that observed in simulating recruitment (b, c, d). Covariates are temperature (left) and stratification index (right). Covariate values are taken from drift trajectories released from the main spawning grounds: (b) Gironde area, (c) Landes area, (d) Capbreton area.